Muon-catalyzed *dd* fusion between 25 and 150 K: Experiment

J. Zmeskal, P. Kammel, A. Scrinzi, W. H. Breunlich, M. Cargnelli, J. Marton, N. Nägele, and J. Werner
Institut für Mittelenergiephysik, Österreichische Akademie der Wissenschaften, Boltzmanngasse 3, A-1090, Vienna, Austria

W. Bertl and C. Petitjean
Paul Scherrer Institut, CH-5232 Villigen, Switzerland
(Received 25 January 1990)

This paper reports an experimental investigation of muon-catalyzed fusion in pure deuterium by detection of *dd* fusion neutrons. Target temperatures of 25.5–150 K and gas densities of 2% and 5% liquid-hydrogen density were used. The rates $\tilde{\lambda}_F$ for $dd\mu$ formation from both hyperfine states of $d\mu$ atoms as well as the hyperfine transition rates $\tilde{\lambda}_{FF'}$ were separated in a kinetic analysis of the observed time spectra. This measurement of the temperature dependence of all important rates in the $dd\mu$ catalysis cycle allows a comprehensive and quantitative test of the present theory of resonant molecule formation. In particular, the temperature behavior of $dd\mu$ formation from the $d\mu$ quadruplet state determines the binding energy $\varepsilon_{11} = -1966.1(3)$ meV of the participating $dd\mu$ state with unique accuracy. In general, convincing agreement between experiment and theory concerning the $dd\mu$ formation process is found, whereas the theoretical hyperfine rates, consisting of nonresonant and resonant contributions, exceed the experimental values by $\sim 40\%$.

I. INTRODUCTION

The discovery of a resonance mechanism in the formation of $dd\mu$ and $dt\mu$ molecules created renewed interest in the question of muon-catalyzed fusion. This resonance process increases the formation rates in the muon catalytic cycle by several orders of magnitude and allows for well above 100 fusions per muon in suitable deuterium-tritium mixtures. Intense research effort is currently concentrated on the understanding of the basic processes of muon catalysis and on the investigation of the effectiveness of this reaction scheme.[1]

Muon catalysis in pure deuterium, the system where the resonance process was found originally, also gained considerable attention due to the following reasons: (a) In view of the difficulties faced in the more complex $dt\mu$ kinetics, the investigation of the prototype $dd\mu$ reaction serves as a guideline for the understanding of the resonance mechanism under well-defined circumstances. (b) Only recently has a complete *ab initio* theory of all important parameters describing the $dd\mu$ system been finished.[2] Experiments are now able to test the theory of the muonic three-body problem with unprecedented accuracy. In particular, the $dd\mu$ binding energy can be determined with extreme precision, testing subtle corrections like QED effects, etc. (c) Experiments on nuclear muon capture in deuterium rely on information about mesomolecular processes for an unambiguous interpretation of the observed rate in terms of basic weak interaction.[3,4]

This paper reports an experimental investigation of muon catalysis processes in pure deuterium in the range $25.5 \leq T \leq 150$ K. The *temperature dependence* of the formation rates for the two hyperfine states of the $d\mu$ atom and the hyperfine transition rates are determined *separately*. In the present work the detailed data analysis as well as the final results and a comparison with other experiments are presented (preliminary results were reported in Refs. 5 and 6). The complete determination of all important kinetic rates in the very sensitive low-temperature range allows the most accurate quantitative test of the theory of $dd\mu$ catalysis processes in pure deuterium. This comparison is subject of a forthcoming paper.[7]

II. MUONIC PROCESSES IN PURE D_2

A. Resonant molecular formation

The basic mechanism of resonant formation has been proposed, calculated, and demonstrated in the pioneering works:[8–10] Given the existence of an extremely weakly bound $dd\mu$ state, $dd\mu$'s can be produced with high rates via the formation of a mesomolecular complex $[(dd\mu)dee]^*$. Contrary to nonresonant formation where the energy excess is transferred to an Auger electron, in this resonance process the $dd\mu$ binding energy is completely used up in the rotational and vibrational excitation of the compound molecule. Since the molecular excitation spectrum consists of discrete levels, resonant formation is possible only for a distinct set of *resonance energies*, i.e., kinetic energies of the initial $d\mu$ atoms. This leads to a strong and characteristic dependence of the molecular formation rates on target temperature.

It took a decade of diligent and worldwide theoretical and experimental efforts to refine this basic scheme into a

quantitative theory (see Ref. 2 and references given therein). After averaging over initial and summing over final rotational states of the participating D_2 and the compound molecule, respectively, the resonant formation process

$$(d\mu)_F + D_2 \longrightarrow [(dd\mu)_S dee]^* \quad (1)$$

can be expressed by partial rates λ_{FS}, which correspond to transitions between the hyperfine substates of the $d\mu$ atom and the $dd\mu$ molecule with total spin F and S, respectively (compare Fig. 1). The highly excited $dd\mu$ state has the rotational and vibrational quantum numbers $J=1$, $v=1$; the compound molecule is formed in a vibrational state with $\nu=7$. Since the hyperfine splittings of the participating $d\mu$ and $dd\mu$ states considerably exceed the available thermal energies (typically some meV at low temperatures), the molecular formation rates from the two $d\mu$ hyperfine states exhibit a very different resonance behavior, as first evidenced in the experiment.[12]

Theoretical efforts concentrated on two questions. On the one hand, it was necessary to accurately define the transition matrix elements for this rearrangement collision and to develop a suitable calculation scheme. A comprehensive treatment of this problem can be found in Ref. 13. On the other hand, for a realistic prediction of the temperature dependence of resonant formation the resonance conditions have to be computed within a fraction of the initial (usually thermal) kinetic energy of the incoming $d\mu$. For the $dd\mu$ binding energy ε_{11} this involves the solution of the muonic three-body problem with the extreme precision of better than 1 meV. Only within the past few years have calculations of the nonrelativistic problem finally reached the required impressive accuracy,[14] whereas calculations of finite-size effects, QED corrections, etc., are still being improved.[1]

B. Back decay and fusion

Owing to exchange symmetry of the $dd\mu$ molecule electric dipole transitions are suppressed in the molecular complex, and the electromagnetic deexcitation cascade is comparatively slow. Hence, back decay into the scattering channel[15]

$$[(dd\mu)_S dee]^* \longrightarrow (\mu d)_{F'} + D_2 \quad (2)$$

successfully competes with dd fusion and Auger deexcitation (see Fig. 2). The back-decay rates $\Gamma_{SF'}$ are given by the rates of the inverse reaction (1) after proper averaging over the rotational states of the molecular complex.

Nuclear fusion proceeds through the channels shown in Fig. 2. Strictly speaking, the fusion rates λ_f and the branching β depend on the quantum numbers of the $dd\mu$ state from which fusion occurs. After resonant formation, fusion takes place nearly exclusively from the $J=1$, $v=1$ state with $\lambda_f = 0.44\times 10^9\ s^{-1}$ (Ref. 16) and $\beta=0.58$ (Ref. 17). This surprising asymmetry between the $n+$He and $p+t$ fusion channel is attributed to the nuclear p-wave interaction in the $J=1$ state. In a $J=0$ state, on the other hand, the nuclear s-wave interaction is expected to lead to a nearly symmetric branching with $\beta=0.5$. Thus for nonresonant formation β varies between 0.5 and 0.58, since $dd\mu$ molecules are populated in both $J=0$ and 1 states there.[18,9]

C. Scattering and hyperfine transition

The quantitative solution of the muonic three-body scattering problem has been developed in the course of muon-catalyzed fusion studies.[19] Since the calculated elastic cross sections are in agreement with a recent experiment[20] and exceed inelastic and molecular formation cross sections by at least one order of magnitude, it is safe to assume (at least in first order) that $d\mu$ atoms are first thermalized to target temperatures before they undergo further reactions (note the different situation in the $dt\mu$ cycle at low densities[21–23]). After thermalization

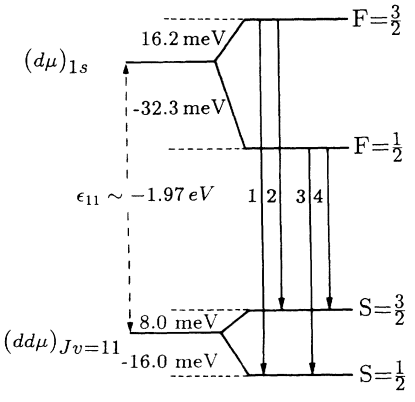

FIG. 1. Hyperfine structure of resonant $dd\mu$ formation. The $d\mu$ and $dd\mu$ hyperfine structure leads to different resonance energies for transitions 1–4. Hyperfine energies for $dd\mu$ have been averaged over additional small splittings due to spin-orbit coupling (Ref. 11).

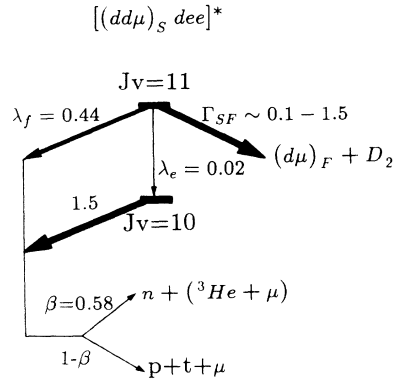

FIG. 2. Decay channels for the mesomolecular complex $[(dd\mu)_{Jv=11} dee]^*$. Back decay (rate Γ_{SF}) competes with fusion (rate λ_f) and the cascade transition to the $dd\mu$ state with $J=1$, $v=0$ (rate λ_e). All rates in units of $10^9\ s^{-1}$.

hyperfine transitions take place by inelastic scattering[24]

$$(\mu d)_{F=3/2}+d \rightleftarrows (\mu d)_{F=1/2}+d \ , \tag{3}$$

where the transition rates $\lambda_{FF'}$ are averaged over the thermal energy distribution of muonic atoms. The two rates $\lambda_{FF'}$ are related by detailed balance

$$\lambda_{1/2\,3/2}=2e^{-\Delta\varepsilon_{d\mu}/kT}\lambda_{3/2\,1/2} \tag{4}$$

with the $d\mu$ hyperfine splitting energy $\Delta\varepsilon_{d\mu}=0.0485$ eV.

D. Kinetics

The basic processes discussed above combine to the experimentally observable kinetics of muon-catalyzed processes.[2] At times large compared to the lifetime $\tau\sim 0.5$ ns of the mesomolecular complex, the kinetics is well described by the scheme of Fig. 3 and primarily depends on the *effective* (i.e., experimentally observable) *molecular formation rates* $\tilde{\lambda}_F$ and the *effective hyperfine transitions rates* $\tilde{\lambda}_{FF'}$. (All collisional rates are normalized to the density $N_0=4.25\times 10^{22}$ cm^{-3} of liquid hydrogen. For comparison with observed experimental rates, these normalized rates have to be multiplied by the relative target density Φ.) Apart from the upwards hyperfine transition $F=\frac{1}{2}\rightarrow F=\frac{3}{2}$, which is ineffective at low temperatures, the kinetics[2] is formally identical with the one used previously in the analysis of experiment[12] and subsequent works. In the recent theory, however, the *interpretation* of the effective rates in terms of basic rates is modified significantly by the effect of back decay.

According to theoretical calculations for the $dd\mu$ excited state, the back-decay rate $\Gamma_S=\sum_F \Gamma_{SF}\sim 1.5\times 10^9$ s^{-1} (Ref. 2) exceeds the rate $\tilde{\lambda}_f=\lambda_f+\lambda_e\sim 0.46\times 10^9$ s^{-1}, which leads to fusion (see Fig. 2, $\lambda_e=0.22\times 10^8$ s^{-1} is the rate of Auger deexcitation[25]). Thus only $\sim\frac{1}{4}$ of the formed $dd\mu$'s are expected to undergo fusion, and the effective molecular formation rates for the two $d\mu$ hyperfine states with spin F are

$$\tilde{\lambda}_F=\lambda_{\rm nr}+\sum_S \lambda_{FS}\frac{\tilde{\lambda}_f}{\tilde{\lambda}_f+\Gamma_S} \tag{5}$$

with parameters $\lambda_1=0.04\times 10^6$ s^{-1} and $\lambda_2=2.3\times 10^6$ s^{-1} eV^{-1} for the nonresonant term[9]

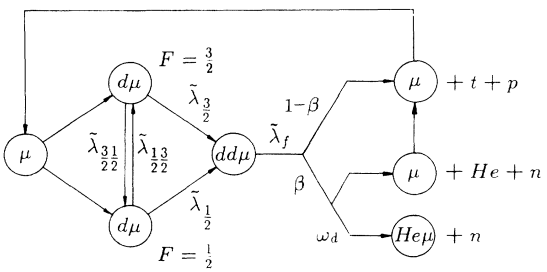

FIG. 3. Simplified $dd\mu$ kinetics.

$$\lambda_{\rm nr}=\lambda_1+\lambda_2\tfrac{3}{2}kT \ . \tag{6}$$

In a similar way, the effective hyperfine transition rate contains a back-decay term due to intermediate formation and subsequent decay of $dd\mu$ molecules[26,2]

$$\tilde{\lambda}_{FF'}=\lambda_{FF'}+\sum_S \lambda_{FS}\frac{\Gamma_{SF'}}{\tilde{\lambda}_f+\Gamma_S} \ . \tag{7}$$

For a deuterium density Φ the kinetics of Fig. 3 corresponds to a system of differential equations with $F=\frac{1}{2},\frac{3}{2}$ $(F\neq F')$

$$\frac{dN_F}{dt}=-\{\lambda_0+\Phi\tilde{\lambda}_F[1-\eta_F(1-\omega)]+\Phi\tilde{\lambda}_{FF'}\}N_F +[\Phi\tilde{\lambda}_{F'}\eta_F(1-\omega)+\Phi\tilde{\lambda}_{F'F}]N_{F'} \ , \tag{8}$$

where η_F are the statistical weights of the $d\mu$ hyperfine states ($\eta_{1/2}=\frac{1}{3}$, $\eta_{3/2}=\frac{2}{3}$) and $\lambda_0=0.455\times 10^6$ s^{-1} is the muon decay rate. For the $n+$He fusion channel the sticking probability to the recoiling He is $\omega_d=0.122(3)$ (Ref. 17), which leads to an average sticking probability per fusion of $\omega=\beta\omega_d$. The resulting time distribution of fusion neutrons consists of two terms proportional to the populations N_F of two $d\mu$ hyperfine states

$$\frac{dn}{dt}=\Phi\sum_F \beta_F\tilde{\lambda}_F N_F \ . \tag{9}$$

In general, β_F is different for the two hyperfine states, since this branching ratio depends on the orbital angular momentum of the $dd\mu$ which is determined by the formation process.

An approximate analytical solution of Eqs. 8 and 9 is

$$\frac{dn}{dt}=\Phi(\beta_{3/2}\tilde{\lambda}_{3/2}-\beta_{1/2}\tilde{\lambda}_{1/2})(\eta_{3/2}-P_{3/2}) \times\exp\left\{-\left[\lambda_0+\Phi\left[\sum_F \tilde{\lambda}_{FF'}+\sum_F \eta_{F'}\tilde{\lambda}_F\right]\right]\right\} +\Phi\sum_F \beta_F P_F\tilde{\lambda}_F\exp\left[-\left[\lambda_0+\Phi\omega_d\sum_F \beta_F P_F\tilde{\lambda}_F\right]t\right] \tag{10}$$

with $F\neq F'$. After the decay of the initial exponential component [first term in Eq. (10)], a steady state between the two $d\mu$ hyperfine states is reached where the relative hyperfine populations P_F ($P_{1/2}+P_{3/2}=1$) are[2]

$$P_{1/2}=(1+\gamma)^{-1} \ \text{ with } \ \gamma=\frac{\tilde{\lambda}_{1/2\,3/2}+\eta_{3/2}\tilde{\lambda}_{1/2}}{\tilde{\lambda}_{3/2\,1/2}+\eta_{1/2}\tilde{\lambda}_{3/2}} \ . \tag{11}$$

III. EXPERIMENT

A. Experimental approach

The main observables in the present experiment were the time distributions dn/dt of 2.45-MeV neutrons, which originate from muon-catalyzed *dd* fusion. As explained above, the observed time structures provide information about the important kinetic rates $\tilde{\lambda}_F$ and $\tilde{\lambda}_{FF'}$.

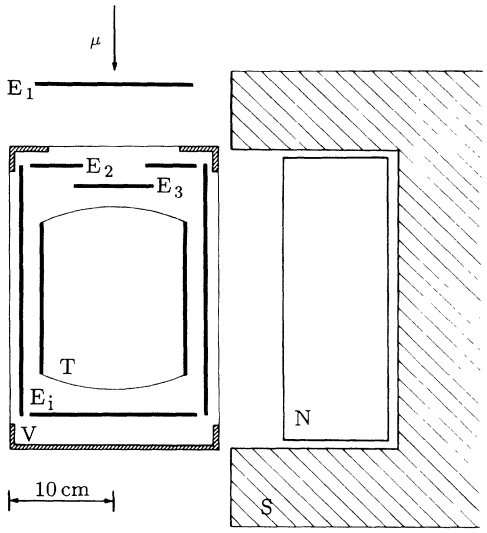

FIG. 4. Experimental setup: target cell (T), vacuum chamber (V), neutron detector (N), muon and electron detectors (E), and paraffin shielding (S).

The investigations cover the low-temperature region $25.5 \leq T \leq 150$ K, where a strong sensitivity to resonance effects was expected.[12] The density range $0.02 \leq \Phi \leq 0.05$ was selected to allow a clear separation of the two components due to the two hyperfine substates of the $d\mu$ atom.

Incoming negative muons were identified by a telescope of plastic detectors and brought to rest in a thin-walled target cell containing high-purity deuterium gas (see Fig. 4). Particles from the subsequent reactions induced by the muons were detected in neutron and electron detectors, including neutrons from fusion and nuclear muon capture as well as electrons from muon decay.

B. Target

The cylindrical target cell of 3200 cm^3 (diameter 14 cm, length ~20 cm, see Fig. 4) consisted of a copper cylinder of 1 mm wall thickness, to which thin Ag entrance windows had been brazed. All inner surfaces of the cell were coated with 0.1 mm of silver. This measure ensured that background from capture neutrons due to wall stops dies away quickly with the short lifetime of μ^- in Ag ($\tau_{Ag}=86$ ns). Since the D_2 fillings correspond to total stopping densities of only 60–120 mg/cm^2, it was crucial to take full advantage of the excellent range width of the low momentum μE4 beam at the Paul Scherrer Institute (PSI, formerly the Swiss Institute for Nuclear Research). Therefore, all material penetrated by the incoming muons was minimized. In particular, the entrance window of the target cell was reduced to 0.5 mm of Ag, just sufficient to safely sustain the maximum operating pressure of 20 bars.

The target cell was contained in an insulation vacuum vessel made of stainless steel. Thin aluminum windows of 1 mm thickness covered the sides of this vessel to reduce neutron scattering. The complete target system is shown schematically in Fig. 5. Cooling was achieved by means of a closed-loop He compressor system and liquid-nitrogen precooling. The temperature setting by resistive heating was controlled by a silicon temperature sensor placed inside the filling line to the target cell. The gas transfer was achieved by a turbomolecular pump and a standard vacuum pump. Special precautions were taken to ensure high gas purity. Baking of the high-vacuum system at 500 K reduced the residual gas pressure to $\leq 10^{-7}$ mbar. Gas filling through a palladium filter reduced impurities to better than 0.01 ppm.

Note that the distribution of ortho- and para-D_2 molecules (i.e., with even and odd rotational quantum numbers) has to be known for the theoretical interpretation of our experiment, since the occupation probability of rotational states enters the calculation of the rates λ_{FS} in Eq. (1) (cf. Refs. 27 and 2). In our target system D_2 molecules were combined in the *statistical mixture* (i.e., ortho to para ratio of 2:1) on the hot Pd surfaces (~500 K), after diffusion of atomic deuterium through the Pd filter. Since ortho-para transitions were negligible in the silver-coated target cell,[28] this statistical ortho-para ratio of D_2 molecules was preserved during the course of the experiment. Hence the population of even and odd rotational states significantly deviated from the equilibrium Boltzmann distribution at low temperatures.

C. Detectors and electronics

The telescope for incoming muons consisted of two coincidence plastic counters E_1, E_3 and several anticoincidence counters E_2, E_i surrounding the target cell. A circular entrance hole in anticounter E_2 of 6 cm diameter determined the final beam spot. The electronic μ stop

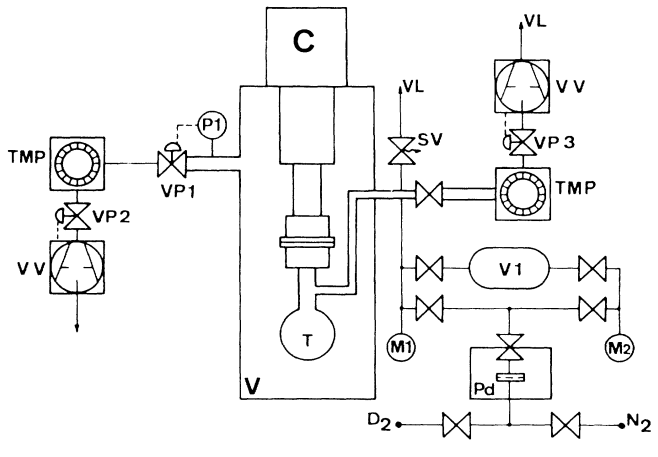

FIG. 5. Target system: target cell (T), cooling unit (*C*) vacuum chamber (V), turbomolecular pump (TMP), forepump (VV), palladium-silver diffusion unit (Pd), 3 l metering volume (V1), bourdon tube gauge (M1,M2), pirani vacuum gauge (P1), pneumatic valve (VP1-3) safety valve (SV), and ventilation line (VL).

TABLE I. Overview of measurements including experimental conditions (Φ, T, and measuring time t), dead-time corrected μ stops $N_\mu \varepsilon_\tau$, results from decay electron analysis (electron disappearance rate λ, intensity N_e, and observed yield per μ stop), and the normalization factor N_n for the observed fusion neutrons.

Data point	Φ	T (K)	t (h)	$N_\mu \varepsilon_\tau$ (units of 10^8)	λ (10^6 s^{-1})	N_e (units 10^8)	$\frac{N_e}{N_\mu \varepsilon_t}$	N_n (units of 10^6)
1	0.0221(3)	25.5(2)	22	4.162	0.452(1)	1.657(16)	0.398(8)	2.241(52)
2	0.0483(5)	40.0(2)	19	3.250	0.452(1)	2.033(20)	0.626(13)	2.639(61)
3	0.0483(5)	70.0(5)	8	1.052	0.454(2)	0.666(7)	0.633(13)	0.864(20)
4	0.0221(3)	70.0(5)	22	4.124	0.455(1)	1.628(16)	0.395(8)	2.201(51)
5	0.0216(3)	95.0(5)	8	0.852	0.455(2)	0.327(3)	0.384(8)	0.442(10)
6	0.0213(3)	117.0(5)	10	1.375	0.455(2)	0.525(5)	0.382(8)	0.710(16)
7	0.0211(3)	150.0(5)	4	1.183	0.455(2)	0.444(4)	0.375(8)	0.599(14)

signal was defined as $E_1 \cdot \bar{E}_2 \cdot E_3 \cdot \overline{\sum_i E_i}$. Electrons from muons decaying in the target were observed by detectors E_2 and E_i placed inside the insulation vaccum vessel. Neutrons were detected by a specially developed liquid scintillation detector (volume $28 \times 14 \times 10$ cm^3, scintillator NE213) (Ref. 29) which combines high efficiency with good pulse shape (PS) discrimination between neutrons and the intense background from bremsstrahlung quanta associated with decay electrons. Target electrons impinging directly on the neutron counter were vetoed by the electron counters E_t.

The electronic logics of this experiment is similar to the one in our previous work.[12] For all events a wide pile-up rejection of ± 14 μs was required against second-beam muons. The following parameters were written on tape: pulse height (E), pulse shape (PS), time between μ stop and neutron ($T_{\mu-n}$), and time between neutron and electron (T_{n-e}) for the neutron detector; time between μ stop and electron ($T_{\mu-e}$) for the electron detectors.

D. Measurements

The measurements were performed at the μE4 beam line of PSI. For an accurate relative measurement it was important to explore different target conditions *consecutively without any change* of the experimental geometry. Two densities $\Phi = 0.02$ and 0.05 were investigated, where the use of the lower density was necessary to prevent liquefaction at $T = 25.5$ K and to stay within the operating pressure of the target at higher T. For both densities the beam momentum was optimized for the highest gas stop fraction ε_{gas} which was monitored by the intensity of electrons disappearing with the rate λ_0 characteristic for muon decay in deuterium. Optimum beam momenta were found to be 47 MeV/c for $\Phi = 0.05$ and 46 MeV/c for $\Phi = 0.02$, resulting in $\varepsilon_{gas} = 0.76$ and 0.47, respectively. A complete list of the experimental conditions for the main data runs is given in Table I. The gas densities were determined by accurate volumetric measurements of the fillings as well as by continuous measurements of temperature and pressure during the runs. Auxilliary runs with μ^+ were used for time calibration and for background studies, fillings with Xe gas, where μ^- are quickly captured, simulated conditions of an empty target.[5]

IV. DATA ANALYSIS

A. Data reduction

1. *Electron spectra*

Time spectra of electrons after muon stop ($T_{\mu-e}$) were created for every run and then summed up for the different data points. As a typical example the spectrum obtained for data point 1 (Table I) is shown in Fig. 6. The intensity of electrons from muon decay exceeds the accidental contribution, seen prior to zero time, by several orders of magnitude. These time spectra were fitted with a formula[5] which explicitly accounts for the time structure of accidentals (due to the high probability of observing decay electrons the chance for the detection of accidentals is reduced at later times). Results of this fit are presented in Table I. The observed electron disappearance rates are in agreement with the muon decay rate λ_0. For data points of the same target density excellent stability is achieved. The slight decrease of electrons per

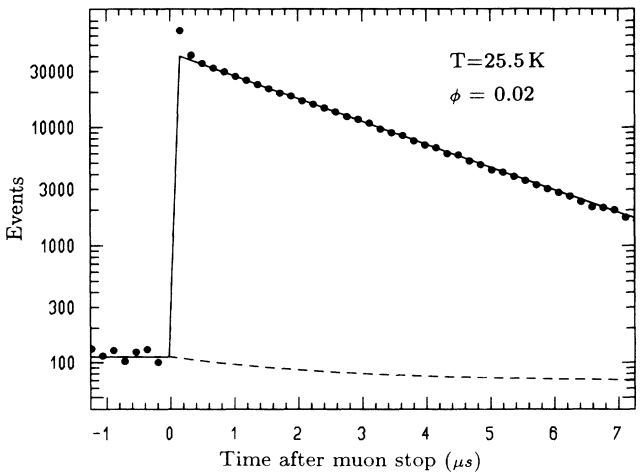

FIG. 6. Time spectrum of electrons after μ^- stop. Solid curve indicates fit of electrons from muon decay in D_2; dashed curve shows shape of accidental background.

μ stop with temperature is consistent with the somewhat smaller target density for these points.

2. *Neutron spectra*

Two-dimensional neutron spectra of energy E versus time $T_{\mu-n}$ were created with a cut on the pulse shapes to select neutrons. Clean fusion neutrons were selected by requiring a delayed electron after the neutron with $T_1 \leq T_{n-e} \leq T_2$ ($T_1 = 0.24$ μs, $T_2 = 3.8$ μs). This condition leads to a dramatic suppression of the most severe background sources. In the process of muon-catalyzed fusion the μ^- *survives* and eventually gives rise to an electron from muon decay. On the contrary, in the capture reaction by weak interaction with nuclei of the D_2 gas or the target walls, the μ^- is *consumed.* Thus, delayed electrons after capture neutrons are due to accidental coincidences only. A resulting suppression of capture neutrons of more than 300 was observed in empty-target runs. Consequently, already after 0.3 μs the fast-decaying component of neutrons from stops in the Ag windows accounts only for $\leq 2\%$ of the fusion spectra with delayed electron coincidence. A similar suppression is obtained for background (γ rays, photoneutrons) produced by decay electrons. The delayed-electron condition leads also to optimal signal-to-accidental ratios. Differently from the processes mentioned above, the observed accidental neutrons are uncorrelated to the decay electrons. This induces a time dependence of the accidental term (due to the time-dependent probability to observe a delayed decay electron after an accidental neutron).[5] After proper normalization the accidental term was subtracted from the fusion spectra (Fig. 7). These accidental terms usually account for less than 10% of the slow time component of fusion neutrons.

No further corrections had to be applied to the fusion spectra. A quantitative understanding of the recoil spectrum from the 2.45-MeV fusion neutrons was achieved, as demonstrated by the agreement between the observed spectrum and a Monte Carlo simulation (Fig. 8). For the final time spectra of fusion neutrons an energy threshold of 340 keV equivalent electron energy was chosen. These spectra are shown for several data points in Fig. 9.

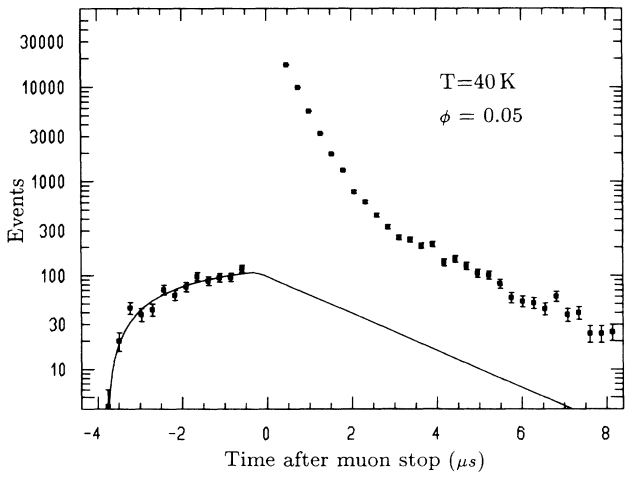

FIG. 7. Raw spectrum of fusion neutrons with delayed electron coincidence. After normalization to the accidental neutrons observed before muon stop (-2.5 μs $\leq T_{\mu-n} \leq -0.8$ μs), the accidental term (solid curve) was subtracted.

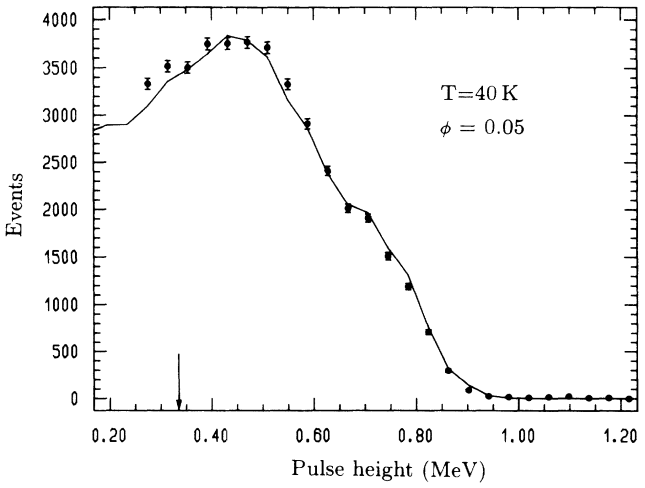

FIG. 8. Observed pulse-height spectrum for 2.45-MeV neutrons from muon-catalyzed *dd* fusion shows good agreement with Monte Carlo simulation of detector response (solid curve). Abscissa calibrated in equivalent electron energy. The energy threshold of 340 keV used in the analysis is indicated by an arrow.

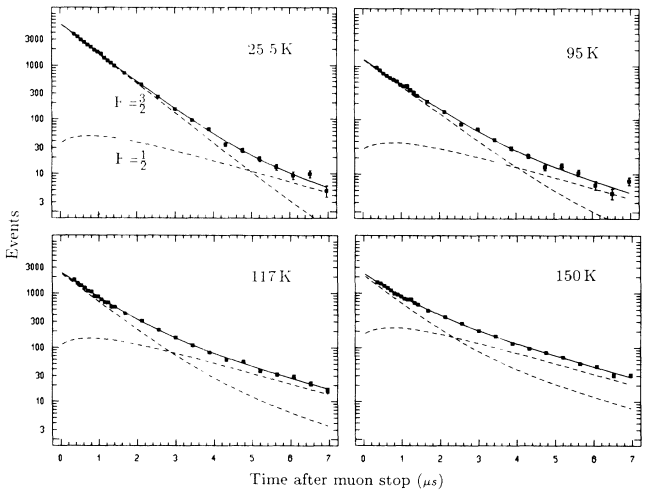

FIG. 9. Selected time spectra of fusion neutrons after muon stop. Target density $\Phi = 0.02$. In the kinetic fits the total neutron rate dn/dt is decomposed into contributions from the two $d\mu$ hyperfine states. The qualitative behavior of the kinetic rates can be read off this figure: molecular formation from the $F = \frac{3}{2}$ state dominates at low T, then the difference between the two contributions decreases with rising T. The slope of the first component which is mainly due to the hyperfine transition rate, remains nearly constant.

B. Relative normalization and stability

The observed time spectra of electrons from μ decay $e_\mu(t)$ (slow component in Fig. 6) and fusion neutrons $n_{\text{coinc}}(t)$ with the requirement of a delayed electron between $T_1 \le T_{\mu-n} \le T_2$ (Fig. 9) can be expressed as

$$e_\mu(t)=N_e\lambda_0 e^{-\lambda_0 t}\ ,$$
$$n_{\text{coinc}}(t)=N_n\frac{dn}{dt}\ , \tag{12}$$

where dn/dt is the theoretical time distribution of fusion neutrons (cf. Sec. II D). The normalization constants are

$$N_e=N_\mu\varepsilon_{\text{gas}}\varepsilon_\tau\varepsilon_e\ ,$$
$$N_n=N_\mu\varepsilon_{\text{gas}}\varepsilon_\tau\varepsilon_e\varepsilon_n\int_{T_1}^{T_2}\lambda_0 e^{-\lambda_0 t}dt\ . \tag{13}$$

Here N_μ is the number of electronic μ stops, ε_{gas} is the fraction of gas stops, $\varepsilon_\tau \sim 0.9$ a correction for the dead time of the data-taking system, and ε_e and ε_n the efficiencies for electron and neutron detection, respectively. From this equation follows immediately

$$N_n=\varepsilon_n N_e(e^{-\lambda_0 T_1}-e^{-\lambda_0 T_2})\ , \tag{14}$$

i.e., the normalization constant for the coincidence neutron spectra is the product of the neutron detection efficiency, the total observed decay electron intensity, and a trivial time gate factor. This relation is the essence of the *coincidence method* employed in the present work for a precise evaluation of the *relative* normalization factors $N_n(\Phi,T)$ between the different data points, a crucial requirement for the accurate determination of the resonant T dependence of molecular formation rates.

Since the coincident fusion spectra are normalized to the number of decay electrons measured simultaneously, electronic inefficiencies and dead time, dominated by the overall CAMAC readout time, cancel completely. The remaining error contributions to N_n were estimated as follows: $\Delta\varepsilon_n/\varepsilon_n=\pm 2\%$ was determined from the stability of the position of the recoil edge in the pulse-height distribution (Fig. 8) and from the stability of the capture neutron intensity per μ stop from wall stops. The error also includes an uncertainty due to the slightly different muon stop distributions for gas densities of 0.02 and 0.05 as calculated by Monte Carlo simulations. The error $\Delta N_e/N_e=\pm 1\%$ results from statistics and the zero-time uncertainty of the $T_{\mu-e}$ circuit. The stability of zero time for the different time circuits was found to be $\Delta T_{\mu-n}=\pm 14$ns, $\Delta T_{\mu-e}=\pm 15$ns, and $\Delta T_{n-e}=\pm 30$ns, respectively.[5] The latter result leads to a relative error of the time gate factor of 1.4%. Altogether, we arrive at an integral uncertainty of 2.6% for N_n. Within the different data points this essential error estimation could be verified directly: The intensity of coincident fusion neutrons per decay electron was evaluated run by run and remained stable within 2%.

C. Absolute normalization

The absolute normalization was determined from results of experiment[4] in pure deuterium of $T=45$ K and $\Phi=0.04$,

$$\tilde{\lambda}_{3/2}=3.74(25)\times 10^6\ \text{s}^{-1}\ ,$$
$$\tilde{\lambda}_{1/2}=0.0449(33)\times 10^6\ \text{s}^{-1}\ . \tag{15}$$

That experiment, aimed primarily at measuring the rate of nuclear muon capture in deuterium, was specifically optimized and carefully analyzed to obtain an accurate absolute rate determination. For the normalization procedure we made use of the final fits to the observed time spectra (cf. Sec. V). It follows from these fits that the temperature dependence of $\tilde{\lambda}_{3/2}$ between 40 and 45 K is very small. Therefore, the value of $\tilde{\lambda}_{3/2}$ for our data point 2 at $T=40$ K was equated to the value of $\tilde{\lambda}_{3/2}$ from Eq. (15) to determine the *absolute* value of $N_n(T=40)=2.64(22)\times 10^6$. The error of N_n consists of the error of the absolute measurement and of the error of $\lambda_{3/2}$ ($T=40$ K) relative to the other data points. This absolute error of 8.4% has to be applied to the complete set of normalization values N_n in Table I as a whole. (Using the small temperature dependence of the nonresonant rate $\tilde{\lambda}_{1/2}$ at low temperatures, a completely consistent alternative absolute normalization is obtained by identifying the values of $\tilde{\lambda}_{1/2}$ instead of $\tilde{\lambda}_{3/2}$ between 40 K and 45 K.) From Eq. (14) we evaluate a neutron detection efficiency $\varepsilon_n=0.0181(15)$ in good agreement with $\varepsilon_n=0.0176(26)$ obtained from a Monte Carlo simulation of our experimental geometry (threshold 340 keV electron energy, distance of 27.8 cm between target and detector center).

D. Target purity

For the final fits of the observed spectra of fusion neutrons the rate of muon disappearance from the fusion cycle has to be known. An increase of this rate might originate from the diffusion of $d\mu$ atoms to the target walls or from transfer to impurities. Diffusion to the Ag surfaces as well as transfer to high-Z impurities is limited to below 1% of λ_0 by the agreement of the slopes in the electron spectra with λ_0 (see Table I), since these processes always imply a corresponding increase of the electron disappearance rate. Transfer to low-Z impurities with an effective rate $\Lambda_{dZ}=\Phi c_Z\lambda_{dZ}$ ($\lambda_{dZ}\sim 10^{11}\ \text{s}^{-1}$), however, is harder to detect, since the muon capture rates $\Lambda_Z \ll \lambda_0$ and electron spectra are not strongly affected. In this case, the neutron rate due to nuclear muon capture is a sensitive probe for all transfer processes, since—even in low-Z elements like C, N, and O—capture is faster by at least two orders of magnitude than capture in deuterium. Thus muon transfer changes the intensity as well as the time distribution of capture neutrons. For an experimental check of transfer to impurities, time spectra of capture neutrons (with energies higher than those of fusion neutrons) were analyzed for all data points, similar to the analysis.[4] At temperatures larger than 70 K the observed intensity of capture neutrons nearly doubles, which might indicate increased outgasing from the target walls. Quantitatively, including conservative error estimates for absolute efficiencies, this increase is compatible with

$\Lambda_{dZ}=0.007(7)\times10^6$ s^{-1}, which corresponds to a minor contamination of $c_z \leq 3$ ppm.

V. KINETIC ANALYSIS OF OBSERVED TIME DISTRIBUTIONS

A. Kinetic model and fit strategy

The observed time distributions of fusion neutrons in Fig. 9 clearly show two components, which—in first order—can be interpreted simply as the contributions from the two $d\mu$ hyperfine states. The short-lived intense component is proportional to the $F=\frac{3}{2}$ population; its intensity determines the molecular formation rate $\tilde{\lambda}_{3/2}$ and its disappearance rate the hyperfine transition rate $\tilde{\lambda}_{3/2\,1/2}$. The absolute intensity of the slow component corresponds to the $F=\frac{1}{2}$ population and fixes the value of $\tilde{\lambda}_{1/2}$. A closer look at the solution of the kinetic equations (sec. II D), however, reveals that (a) an additional rate comes into play by the upwards hyperfine transition rate $\tilde{\lambda}_{1/2\,3/2}$ and (b) the branchings $\beta_F(T)$ depend on the different contributions to the $dd\mu$ formation rate at a given temperature, which are not known *a priori*. Problem (a) is solved readily since it can be proved that not only the scattering part but also the back-decay part in Eq. (7) fulfills an approximate detailed balance relation.[7] Deviations from detailed balance occur only at low T, where $\tilde{\lambda}_{1/2\,3/2}$ is very small compared to the other kinetic rates. Thus Eq. (4) is presupposed for the total rate $\tilde{\lambda}_{FF'}$ as well. Problem (b) is relevant for $\tilde{\lambda}_{1/2}$ only, since $\tilde{\lambda}_{3/2}$ is completely dominated by resonance formation. A nearly theory-independent solution is aimed at by an iterative fit procedure. First, we fit the time distribution of fusion neutrons with a simplified model with *constant* temperature-independent branchings $\beta_{1/2}$. Then, the resulting values of $\tilde{\lambda}_{1/2}$ are used to calculate the ratio of resonant to nonresonant formation at each temperature, which finally determines the values of $\beta_{1/2}(T)$.

B. Fit results and errors

The observed time distributions (cf. Fig. 9) were fitted according to Eqs. (9) and (12) using the *numerical solution* of the kinetic equations Eq. (8). For these initial fits $\beta_{1/2}=0.53$ and $\beta_{3/2}=0.58$ were assumed, and $\tilde{\lambda}_F$ and $\tilde{\lambda}_{FF'}$ were varied. The stability of the results for different fit ranges was studied carefully (start 0.3–1.0 μs, end 7 μs). For data points where some correlation between the results and the fit boundaries was noted the errors of the fit results were increased. The uncertainty of the muon disappearance rate was taken into account explicitly for temperatures above 70 K. After this, systematic experimental errors were evaluated (Table II). The total errors of these relative rate measurements are given by the quadratic sum of the three contributions presented in Table III. The consistency between the results at different densities was verified between data points 3 and 4 taken at an identical temperature of 70 K:

$$\begin{aligned}&\Phi=0.0483,\ \tilde{\lambda}_{1/2}=0.0760(45),\ \tilde{\lambda}_{3/2}=3.61(20),\ \tilde{\lambda}_{3/2\,1/2}=34.2(1.1);\\&\Phi=0.0221,\ \tilde{\lambda}_{1/2}=0.0786(65),\ \tilde{\lambda}_{3/2}=3.74(21),\ \tilde{\lambda}_{3/2\,1/2}=36.0(1.7),\end{aligned}\tag{16}$$

where all rates are given in units of 10^6 s^{-1}. Finally, it should be remembered that $d\mu$ atoms may not be thermalized at very early times. Compared to the kinetics equation (8) this leads to a ~10-ns delay in the depopulation of the upper hyperfine state at $\Phi=0.02$.[30] This effect is ignored in the present analysis of the relative rate behavior, since it depends on processes at high energies compared to the target temperatures and is thus similar for all investigated temperature conditions.

For the final correction to $\tilde{\lambda}_{1/2}$ a value of $\lambda_{nr}\sim0.046\times10^6$ s^{-1} was derived from the flat nonresonant part of the observed rates $\tilde{\lambda}_{1/2}$ at $T\lesssim40$ K (see

TABLE II. Systematic errors of the relative rate measurement.

Source of error	Amount	Resulting error of observed rates in % $\Delta\tilde{\lambda}_{1/2}$	$\Delta\tilde{\lambda}_{3/2}$	$\Delta\tilde{\lambda}_{3/2\,1/2}$
Density Φ	1.5%	1.5	1.5	1.5
Temperature	0.2 K (20–50 K) 0.5 K (50–150 K)	1.0	1.0	0.5
Time zero $T_{\mu-n}$	14 ns	0.6	2.5 ($\Phi=0.05$) 1.2 ($\Phi=0.02$)	1.0
Time calibration	1%	1.0	1.0	1.0
N_n	2.6%	2.6	2.6	
Accidental subtraction		3.5 ($T<26$ K) <2 ($T>26$ K)		
Capture neutron subtraction		1.5	1.0	0.5
Sum		5.1 ($T<26$ K) 4.2 ($T>26$ K)	4.3 ($\Phi\sim0.05$) 3.6 ($\Phi\sim0.02$)	2.2

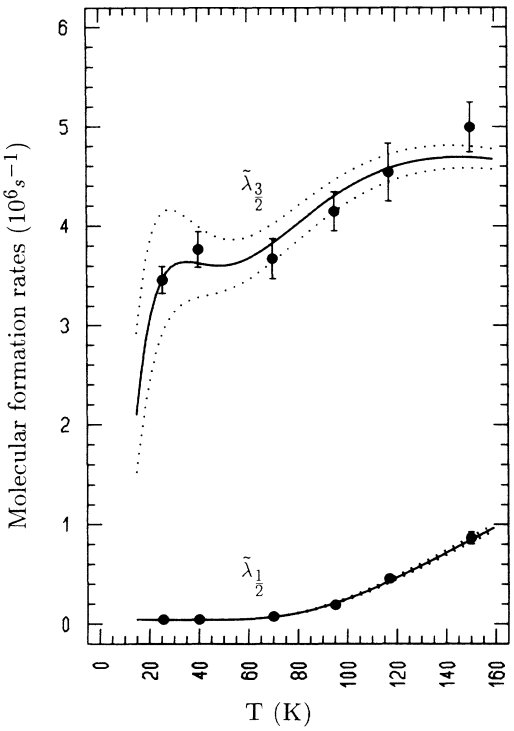

FIG. 10. Molecular formation rates $\tilde{\lambda}_F$. The experimental errors shown do not include the 8.4% uncertainty in the absolute normalization of the whole data set. Solid curve represents best-fit results according to Table VI. The region between dotted curves corresponds to a variation of $\varepsilon_{11}\pm 0.5$ meV from best-fit value.

Fig. 10). The fraction of resonant formation is then estimated on the basis of the *observed* rates $\tilde{\lambda}_{1/2}(T)$ to determine

$$\beta_{1/2}(T)=\frac{\lambda_{nr}}{\tilde{\lambda}_{1/2}}\beta_{nr}+\left[1-\frac{\lambda_{nr}}{\tilde{\lambda}_{1/2}}\right]\beta_r\ , \tag{17}$$

with $\beta_{nr}=0.53(1)$ and $\beta_r=0.580(5)$. The only model dependence of this procedure is contained in the estimate for β_{nr} [arrived at by assuming that at low T nonresonant formation populates $J=0$ and $J=1$ $dd\mu$ states with a ratio of 2:1 (Ref. 9)] and by the use of a constant value for λ_{nr}. To achieve partial independence from these assumptions, the errors of the final $\beta_{1/2}$ (Table IV) were enlarged to cover also the possibility of a nonresonant term according to Eq. (6).

With these values for $\beta_{1/2}(T)$ determined experimentally, the complete set of time distributions was fitted again. The resulting final values of $\tilde{\lambda}_F$ and $\tilde{\lambda}_{3/2\,1/2}$ are presented in Table V. The final errors are the quadratic sum of the errors discussed above (Table III) plus the uncertainties of $\beta_{1/2}(T)$.

VI. RESULTS AND DISCUSSION

A. Molecular formation

The molecular formation rates $\tilde{\lambda}_{1/2}$ and $\tilde{\lambda}_{3/2}$ from the two $d\mu$ hyperfine states show a strikingly different temperature behavior (see Fig. 10). Owing to low-energy resonances, $\tilde{\lambda}_{3/2}$ is particularly sensitive to the exact location of the resonance energies, since the spread of thermal $d\mu$ energies, which tends to smear out the resonance structures, decreases with T. For a quantitative analysis, a fit program was developed to calculate effective molecular rates $\tilde{\lambda}_F$ using the formalism and formation matrix elements of Menshikov *et al.*[2,13] In our calculations statistical ortho-para distribution of D_2 was assumed, which is the adequate description of the experimental situation (cf. Sec. III B). At the low densities and temperatures of our experiment also the competition between rotational relaxation[31] and back decay of the mesomolecular complex had to be taken into account [this leads to some modifications of the simplified expressions for the effective rates Eqs. (5) and (7), as discussed in Ref. 7]. These calculated rates were then simultaneously fitted to all observed rates $\tilde{\lambda}_F$ to determine the nonresonant formation rates λ_1, the effective fusion rate $\tilde{\lambda}_f$, and the $dd\mu$ binding energy ε_{11} (see Sec. II). The results of these fits are compared with most recent theoretical results in Table VI, a detailed discussion of this analysis will be

TABLE III. Comparison of different contributions to the total error of the relative rate measurments. For every point and every observed rate, the error from the fit of the time spectra is given in column (a), the error due to the uncertainty in the muon disappearance rate and due to the sensitivity to the fit range is given in column (b), and the systematic experimental errors in column (c).

		Error contributions (%)								
Data		$\Delta\tilde{\lambda}_{1/2}$			$\Delta\tilde{\lambda}_{3/2}$			$\Delta\tilde{\lambda}_{3/2\,1/2}$		
point	T (K)	(a)	(b)	(c)	(a)	(b)	(c)	(a)	(b)	(c)
1	25.5	10	0.0	5.1	1.4	0.0	3.6	1.7	0.0	2.2
2	40	2.6	0.0	4.2	2.0	0.0	4.3	1.2	0.0	2.2
3	70	3.5	0.0	4.2	3.5	0.0	4.3	2.4	0.0	2.2
4	70	6.8	0.0	4.2	1.5	4.0	3.6	1.8	3.6	2.2
5	95	9.9	4.8	4.2	3.1	0.0	3.6	4.7	0.0	2.2
6	117	4.2	5.3	4.2	2.9	4.5	3.6	4.8	5.5	2.2
7	150	3.0	4.8	4.2	3.6	0.0	3.6	6.7	2.8	2.2

TABLE IV. Branching ratio $\beta_{1/2}(T)$ determined with the help of experimental $dd\mu$ formation rates.

T (K)	$\beta_{1/2}$
25.5	0.530(21)
40	0.530(21)
70	0.550(22)
95	0.568(26)
117	0.575(20)
150	0.578(20)

presented in a subsequent paper.[7]

The most remarkable result is the experimental determination of the $dd\mu$ binding energy with an extreme accuracy of 0.3 meV, which corresponds to 10^{-7} of the muonic Rydberg energy. This error is the quadratic sum of the fit error (0.16 meV) and a contribution (0.25 meV) resulting from estimated uncertainties in the theoretical analysis. The strong sensitivity of $\tilde{\lambda}_{3/2}$ to a variation of ε_{11} is demonstrated in Fig. 10. Agreement between the experimental value and the most recent calculations of ε_{11} has reached ~ 1 meV. At this level subtle corrections to the three-body bound-state problem can already be verified, in particular the calculated energy shift of ~ 9 meV due to vacuum polarization (cf. Ref. 1). For nonresonant $dd\mu$ formation we used a constant term in our final fit since no strong indication for the term linear in energy is present in our data [a fit according to Eq. (6) gives $\lambda_2 \leq 0.85\times 10^6$ eV^{-1}s^{-1}]. Concerning the effective fusion rate $\tilde{\lambda}_f$ it is important to realize that the back-decay factor in Eq. (5) induces a strong correlation between the magnitude of the $dd\mu$ formation matrix elements and $\tilde{\lambda}_f$. Thus we stress that—different from the other experimental results presented here—the extracted value for $\tilde{\lambda}_f$ in Table VI significantly depends on the absolute size of the matrix elements[13] used in our fit (the sensitivity of our fit results to the theoretical input is investigated in Ref. 7).

The results of this work are compared to other experimental data in Fig. 11. Note that two distinct sets of observed rates are shown, corresponding to the different contributions from the two $d\mu$ hyperfine states.

(a) In our systematic studies (this experiment and Refs. 12, 4, and 32) the rates $\tilde{\lambda}_F$ from the two $d\mu$ hyperfine states were determined separately. The earlier result[12] reporting the ratio $\tilde{\lambda}_{3/2}/\tilde{\lambda}_{1/2}$ at $T=34.8$ K was normalized in the same way as described in Sec. IV C. It is obvious from Fig. 11 that the different measurements are consistent with the present data as well as with the best theoretical fit. The results of experiment[32] performed with liquid deuterium ($\Phi=1.15$, $T=23.8$ K) agree within error with the measurements in gas targets ($0.02 \leq \Phi \leq 0.08$).

(b) Experiments (Refs. 10, 17, 33, 34, and 35) present their results in terms of a *single overall* $dd\mu$ formation rate, without distinguishing between the contributions from the two basic rates $\tilde{\lambda}_{1/2}$ and $\tilde{\lambda}_{3/2}$. This description is an oversimplification and hence a rigorous comparison with basic theory and with our experimental results is not always possible. In a reasonable approximation, however, the majority of these measurements can be described by the steady-state molecular formation rate

$$\tilde{\lambda}_{dd\mu}=\sum_F P_F \tilde{\lambda}_F \ , \tag{18}$$

which is an average over the relative population P_F of the two $d\mu$ hyperfine states in the steady state [cf. Eq. (11)]. As seen in Fig. 11, a calculation of $\tilde{\lambda}_{dd\mu}$ based on the best-fit values from the present analysis (Table VI) gives fair agreement with most of the data points of experiments.[17,33,34,35] This agreement deteriorates at low temperatures. There, $\tilde{\lambda}_{3/2} \gg \tilde{\lambda}_{1/2}$ and the observed formation rates critically depend on the contribution from the $(d\mu)_{F=3/2}$ population which is quantitatively identified only in our results. The pioneering experiment of Bystritskii *et al.*[10] seems to have a normalization problem, since a similar T dependence is found, but the rates are by a factor of ~ 4 smaller than in all subsequent experiments (this discrepancy was first demonstrated by Balin *et al.*[17]). In experiments by Jones *et al.*[33] $dd\mu$ formation rates were derived from loss terms measured in DT mixtures. Their theoretical interpretation is difficult, since—in this case—$d\mu$ hyperfine populations P_F are not determined by Eq. (11), but depend on details of the $dt\mu$ cycle.[21] According to the kinetic rates determined in the present work, the result of Balin *et al.* at 293 K (Ref. 17) can be interpreted unambiguously as the steady-state rate defined in Eq. (18). Its value $\tilde{\lambda}_{dd\mu}=2.76(8)\times 10^6$ s^{-1}

TABLE V. Final results $\tilde{\lambda}_F$ and $\tilde{\lambda}_{3/2\,1/2}$ from the relative rate measurements. An absolute calibration error has to be applied to the data set as a whole. This additional error is 8.4% for $\tilde{\lambda}_F$ and 1% for $\tilde{\lambda}_{3/2\,1/2}$, respectively.

T (K)	$\tilde{\lambda}_{1/2}$ (10^6 s^{-1})	$\tilde{\lambda}_{3/2}$ (10^6 s^{-1})	$\tilde{\lambda}_{3/2\,1/2}$ (10^6 s^{-1})
25.5	0.0468(54)	3.46(13)	36.0(10)
40.0	0.0469(25)	3.76(18)	36.8(9)
70.0	0.0769(45)	3.67(20)	34.8(11)
95.0	0.191(23)	4.14(20)	32.7(17)
117.0	0.455(36)	4.54(29)	35.8(27)
150.0	0.864(61)	4.99(25)	37.3(28)

TABLE VI. Parameters of $dd\mu$ formation. Experimental values are derived from a fit of the observed molecular formation rates $\tilde{\lambda}_F$ (Fig. 10) with the theoretical model (Ref. 7). If complete rotational relaxation of the formed mesomolecular complex is assumed (Ref. 2), ε_{11} changes slightly to -1965.9 meV.

Parameter	This experiment	Theory
ε_{11} (meV)	$-1966.1(3)$	$-1965.4, -1966.8$[a]
λ_1 (s^{-1})	$4.60(44)\times 10^4$	4×10^4 [b]
$\tilde{\lambda}_f$ (s^{-1})	$3.1(4)\times 10^8$	4.6×10^8 [c]

[a] cf. Ref. 1.
[b] Reference 18.
[c] References 16 and 25.

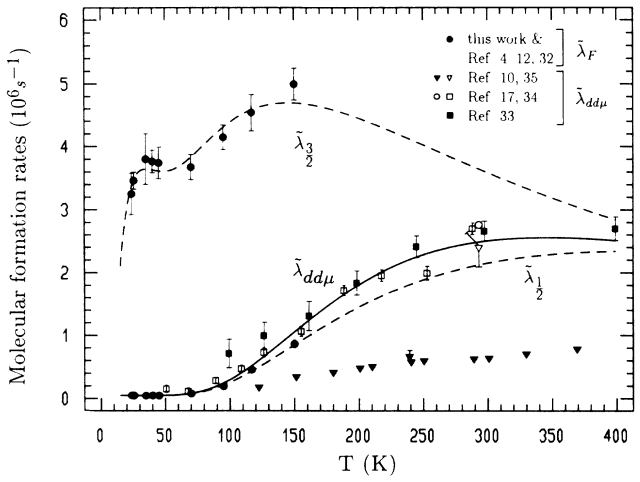

FIG. 11. Comparison of experimental $dd\mu$ formation rates for $T \leq 400$ K. Two classes of experiments are displayed: measurements of the hyperfine formation rates $\tilde{\lambda}_{1/2}$ and $\tilde{\lambda}_{3/2}$ [closed circles: this experiment and our earlier experiments (Refs. 4, 12, and 32)] and measurements of the average molecular formation rates $\tilde{\lambda}_{dd\mu}$, mainly corresponding to the steady state situation [Bystritskii *et al.* (Refs. 10 and 35), Balin *et al.* (Refs. 17 and 34), and Jones *et al.* (Ref. 33)]. Theoretical curves ($\tilde{\lambda}_F$ dashed, $\tilde{\lambda}_{dd\mu}$ solid) were calculated with best-fit parameters from Table VI.

is $\sim 10\%$ larger than the corresponding $\tilde{\lambda}_{dd\mu}$ extrapolated from our results at $T \leq 150$ K, but the error bars of the two experiments overlap (the uncertainty of the extrapolated curves is at least 8.4%, i.e., the absolute normalization error of the $dd\mu$ formation rates given in Table V). Finally, we point out that also the early bubble chamber data[36] on $dd\mu$ formation (not shown in Fig. 11) can be reconciled with theory and the recent counter experiment in liquid D_2, if their results are interpreted correctly as the total yield from both $d\mu$ hyperfine states (see Ref. 32).

In conclusion, after slight adjustments of the basic parameters ε_{11} and $\tilde{\lambda}_f$ to fit the rates $\tilde{\lambda}_F$ observed in the present experiment, current theory of resonant $dd\mu$ formation is found to describe all measured $dd\mu$ formation rates between 23 and 400 K with an accuracy of a few percent.

B. Hyperfine transitions

In this work the temperature dependence of $d\mu$ hyperfine transitions was measured (see Fig. 12). This information is of particular interest because the resonance structure of the back-decay term in Eq. (7) (due to the formation rates λ_{FS}) should be directly visible in the T dependence of the effective hyperfine transition rate $\tilde{\lambda}_{3/2\,1/2}$. Indeed, there is some evidence for such a structure in the shape of the data, but no quantitative agreement with theory. The theoretical scattering rate[24] is close to the total rate $\tilde{\lambda}_{3/2,\,1/2}$ observed in this experiment and therefore does not leave much room for an additional contribution from back decay. However, its flat variation with T does not reproduce the data very well. When the back decay term is added, the total theoretical curve significantly exceeds the experimental points, but shows a similar T dependence.

Figure 12 indicates good consistency between the present results and our other previous measurements of $\tilde{\lambda}_{3/2\,1/2}$ in gaseous targets. The rate in liquid D_2 at 23.8 K (Ref. 32) is smaller by a factor of 0.85(3) than our neighboring gas point measured at 25.5 K. Such a steep decrease cannot be explained by the resonant T dependence of the back-decay term alone and, hence, might be an indication for some density dependence of the hyperfine transition rate $\tilde{\lambda}_{3/2\,1/2}$.[7]

It is evident from Fig. 12 that several results obtained in independent experiments[4,12,32] are consistently smaller by $\sim 40\%$ than the total theoretical rate $\tilde{\lambda}_{3/2\,1/2}$ for $d\mu$ hyperfine transitions, which consists of one term due to scattering and a second one due to resonant $dd\mu$ formation with subsequent back decay (see Fig. 12). Since an error of this magnitude is hardly conceivable in the measurement of the slope in the experimental time distribution under consideration here (see Sec. V), at least one of the two contributions to the theoretical rate $\tilde{\lambda}_{3/2\,1/2}$ seems to be smaller than calculated. The resonant back-decay contribution in Fig. 12 was calculated with the best-fit parameters (Table VI) and the theoretical matrix

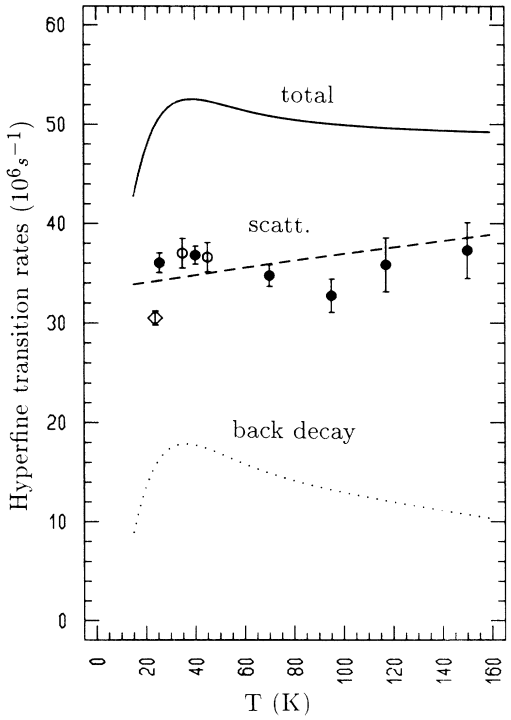

FIG. 12. Hyperfine transition rate $\tilde{\lambda}_{3/2\,1/2}$. Gaseous D_2: closed circles (this experiment), open circles (Refs. 12 and 4), liquid D_2: open diamonds (Ref. 32). The total calculated rate (solid line), which consists of contributions from scattering [dashed line; calculation (Ref. 24) and back decay (dotted line), disagrees with the experimental points in magnitude while showing a similar T dependence.

elements for $dd\mu$ formation.[13] No additional free parameters were used. A reduction of this contribution would imply smaller values of these matrix elements, on which this rate strongly depends [compare Eq. (7) and the discussion in Ref. 7]. As another possibility the theoretical scattering rate $\lambda_{3/2\,1/2}$ may account for the disagreement. Although the accuracy of a recent calculation of this rate is estimated to be better than 10%,[24] all calculations up to now have been performed for bare nuclear targets, and not for D_2 molecules. Thus, calculations incorporating molecular structure and screening effects would be extremely desirable. In particular, reliable theoretical information on the T dependence of the scattering part would allow the separation of the back-decay component in the observed rate $\tilde{\lambda}_{3/2\,1/2}$. As discussed above, the size of this rate would provide direct experimental information about the magnitude of the matrix elements of resonant $dd\mu$ formation.

C. Concluding remarks

During the last decade combined experimental and theoretical efforts have tried to unveil a microscopic picture of muon induced reactions in mixtures of hydrogen isotopes. This effort was motivated by the interest in few body reactions in the presence of both Coulomb and strong forces as well as in weak capture processes. Last but not least, the $dd\mu$ and $dt\mu$ molecules hold an eminent position in the context of muon-catalyzed fusion research. They are the only muonic molecules where the resonant formation process, which is responsible for the large fusion yields in deuterium-tritium mixtures, can be studied.

The measurement of the essential kinetic rates in deuterium gas at low temperatures presented in this work provides a crucial step towards the above mentioned goals. At low temperatures resonance structures are sharply defined, because the spread of thermal energies is small. Moreover, the most intense transitions for resonant $dd\mu$ formation from the $d\mu$ quadruplet state are located just at these temperatures. Hence the formation rates $\tilde{\lambda}_F$ from the two $d\mu$ hyperfine states with spin $F=\frac{1}{2}$ and $\frac{3}{2}$, respectively, differ strongly and could be clearly separated in the observed time spectra of fusion neutrons. These rates as well as the hyperfine transition rate $\tilde{\lambda}_{3/2\,1/2}$ were determined accurately as a function of temperature. Regarding molecular formation a quantitative comparison of the rates $\tilde{\lambda}_F$ from this experiment and *ab initio* theory is possible, and convincing agreement has been found. Above all, this agreement constitutes an important verification of three-body bound-state calculations. The binding energy ε_{11} of the $dd\mu$ state, which participates in resonant formation, is determined experimentally in a nearly model independent way and coincides within 1 meV with recent theoretical calculations. The experimental test of the theoretical formation matrix elements is less stringent, since the observed formation rates depend not only on the $dd\mu$ formation process, but also on the subsequent competition between back decay and fusion. Additional information on these competing decay channels is contained in the observed hyperfine transition rate $\tilde{\lambda}_{3/2\,1/2}$ reported here, since the back-decay contribution to this rate is highly sensitive to the theoretical matrix elements. Unfortunately, at present there is a significant discrepancy between experiment and theory concerning $\tilde{\lambda}_{3/2\,1/2}$ and improvements in the quantitative theoretical description of hyperfine transitions are still required. In summary, however, the present comprehensive set of observed kinetic rates establishes an almost complete picture of the $dd\mu$ cycle, which basically is consistent with current theoretical understanding.

ACKNOWLEDGMENTS

Support by the Austrian Science Foundation and the Paul Scherrer Institute is gratefully acknowledged. We are indebted to Professor Blaser and Professor Lintner for continuous support and encouragement. We are grateful to H. Fuhrmann and P. Pawlek for their participation during data taking. It is a pleasure to thank L. Ponomarev and M. Faifman for many helpful discussions concerning the theoretical analysis, and for providing $dd\mu$ formation matrix elements prior to publication. Finally our thanks are due to the PSI technical staff for its excellent assistance.

[1]W. H. Breunlich, P. Kammel, J. S. Cohen, and M. Leon, Annu. Rev. Nucl. Part. Sci. **39**, 311 (1989).

[2]L. I. Menshikov *et al.*, Zh. Eksp. Teor. Fiz **92**, 1173 (1987) [Sov. Phys.—JETP **65**, 656 (1987)].

[3]G. Bardin *et al.*, Nucl. Phys. **A453**, 591 (1986).

[4]M. Cargnelli, Ph.D. thesis, Technical University of Vienna, Vienna, 1986 (unpublished); M. Cargnelli *et al.*, in *Proceedings of the 23rd Yamada Conference on Nuclear Weak Processes and Nuclear Structure, Osaka, 1989,* edited by M. Morita, E. Ejiri, H. Ohtsubo, and T. Sata (World Scientific, Singapore, 1989), p. 115.

[5]J. Zmeskal, Ph.D. thesis, University of Vienna, 1986 (unpublished).

[6]J. Zmeskal *et al.*, Muon Catalyzed Fusion **1**, 109 (1987).

[7]A. Scrinzi *et al.* (unpublished).

[8]E. A. Vesman, Pis'ma Zh. Eksp. Teor. Fiz. **5**, 113 (1967) [JETP Lett. **5**, 91 (1967)].

[9]S. I. Vinitskii *et al.*, Zh. Eksp. Teor. Fiz. **74**, 849 (1978) [Sov. Phys.—JETP **47**, 444 (1978)].

[10]V. M. Bystritskii *et al.*, Zh. Eksp. Teor. Fiz. **76**, 460 (1979) [Sov. Phys.—JETP **49**, 232 (1979)].

[11]D. D. Bakalov, Yad. Fiz. **48**, 335 (1988) [Sov. J. Nucl. Phys. **48**, 210 (1988)].

[12]P. Kammel *et al.*, Phys. Lett. **112B**, 319 (1982), Phys. Rev. A **28**, 2611 (1983).

[13]L. I. Menshikov, T. A. Strizh, and M. P. Faifman, Muon Catalyzed Fusion **4**, 1 (1989).

[14]I. V. Puzynin and S. I. Vinitskii, Muon Catalyzed Fusion **3**, 307 (1988).

[15]A. M. Lane, Phys. Lett. **98A**, 337 (1983).

[16]L. N. Bogdanova *et al*, Phys. Lett. **115B**, 171 (1982); **167B**, 485 (E) (1986).

[17]D. V. Balin *et al.*, Phys. Lett. **141B**, 173 (1984); Pis'ma Zh. Eksp. Teor. Fiz. **40**, 318 (1984)] [JETP Lett. **40**, 1112 (1984)].
[18]L. I. Ponomarev and M. P. Faifman, Zh. Eksp. Teor. Fiz. **71**, 1689 (1976) [Sov. Phys—JETP **44**, 886 (1976)].
[19]V. S. Melezhik, L. I. Ponomarev, and M. Faifman, Zh. Eksp. Teor. Fiz. **85**, 434 (1983) [Sov. Phys—JETP **58**, 254 (1983)].
[20]J. B. Kraiman *et al.*, Phys. Rev. Lett. **63**, 1942 (1989).
[21]W. H. Breunlich *et al.*, Muon Catalyzed Fusion **1**, 67 (1987).
[22]J. S. Cohen and M. Leon, Phys. Rev. Lett. **55**, 52 (1985).
[23]P. Kammel, Nuovo Cimento Lett. **43**, 349 (1985).
[24]L. Bracci *et al.*, Phys. Lett. A **134**, 435 (1989).
[25]D. D. Bakalov *et al.*, Zh. Eksp. Teor. Fiz. **94**, 61 (1988) [Sov. Phys—JETP **67**, 1990 (1988)].
[26]M. Leon, Phys. Rev. A **33**, 4434 (1986).
[27]M. Leon and J. S. Cohen, Phys. Rev. A **31**, 2680 (1985).
[28]P. C. Souers, *Hydrogen Properties for Fusion Energy* (California University Press, Berkeley, 1985), p. 308.
[29]J. Marton *et al.*, in *Proceedings of the International Conference on Nuclear Data for Science and Technology, Antwerp, 1982,* edited by K. H. Böckhoff (Reidel, Dordrecht, 1983), p. 878.
[30]Estimate from a Monte Carlo simulation of the $d\mu$ thermalization kinetics [M. Jeitler (private communication)].
[31]N. T. Padial *et al.*, Phys. Rev. A **37**, 329 (1988); and N. Padial and J. Cohen (private communication).
[32]N. Nägele *et al.*, Nucl. Phys. **A439**, 397 (1989).
[33]S. E. Jones *et al.*, Phys. Rev. Lett. **56**, 588 (1986).
[34]D. V. Balin *et al.*, Muon Catalyzed Fusion **2**, 241 (1988).
[35]V. M. Bystritskii *et al.*, in *Muon-Catalyzed Fusion (Sanibel Island, 1988),* Proceedings of the Conference on Muon-Catalyzed Fusion, AIP Conf. Proc. No. 81, edited by S. E. Jones, J. Rafelski, and H. J. Monkhorst (AIP, New York, 1989), p. 17.
[36]J. Fetkovich *et al.*, Phys. Rev. Lett. **4**, 570 (1960); J. Doede, Phys. Rev. **132**, 1782 (1963).